AGU Advances

RESEARCH ARTICLE
10.1029/2021AV000408

This article is a companion to Thompson (2021), https://doi.org/10.1029/2021AV000533.

Key Points:

- We use a novel Bayesian approach to account for cross-correlations and spatial uncertainties in top-down flux estimates
- We validate and refine bottom-up wetland methane (CH_4) estimates with satellite-informed CH_4 flux estimates
- We find a lower-than-expected sensitivity of global wetland CH_4 emissions to temperature

Supporting Information:

Supporting Information may be found in the online version of this article.

Correspondence to:

S. Ma,
shuang.ma@jpl.nasa.gov

Citation:

Ma, S., Worden, J. R., Bloom, A. A., Zhang, Y., Poulter, B., Cusworth, D. H., et al. (2021). Satellite constraints on the latitudinal distribution and temperature sensitivity of wetland methane emissions. *AGU Advances*, *2*, e2021AV000408. https://doi.org/10.1029/2021AV000408

Received 12 FEB 2021
Accepted 12 JUL 2021

Peer Review The peer review history for this article is available as a PDF in the Supporting Information.

Satellite Constraints on the Latitudinal Distribution and Temperature Sensitivity of Wetland Methane Emissions

Shuang Ma[1], John R. Worden[1], A. Anthony Bloom[1], Yuzhong Zhang[2,3], Benjamin Poulter[4], Daniel H. Cusworth[1], Yi Yin[5], Sudhanshu Pandey[6], Joannes D. Maasakkers[6], Xiao Lu[7,8], Lu Shen[7], Jianxiong Sheng[9], Christian Frankenberg[5], Charles E. Miller[1], and Daniel J. Jacob[7]

[1]Jet Propulsion Laboratory, California Institute of Technology, Pasadena, CA, USA, [2]Key Laboratory of Coastal Environment and Resources of Zhejiang Province, School of Engineering, Westlake University, Hangzhou, China, [3]Institute of Advanced Technology, Westlake Institute for Advanced Study, Hangzhou, China, [4]NASA Goddard Space Flight Center, Biospheric Science Laboratory, Greenbelt, MD, USA, [5]Division of Geological and Planetary Sciences, California Institute of Technology, Pasadena, CA, USA, [6]SRON Netherlands Institute for Space Research, Utrecht, The Netherlands, [7]School of Engineering and Applied Sciences, Harvard University, Cambridge, MA, USA, [8]School of Atmospheric Sciences, Sun Yat-Sen University, Zhuhai, China, [9]Center for Global Change Science, Massachusetts Institute of Technology, Cambridge, MA, USA

Abstract Wetland methane (CH_4) emissions comprise about one-third of the global CH_4 source. The latitudinal distribution and climate sensitivity of wetland CH_4 fluxes are the key determinants of the global CH_4-climate feedback. However, large differences exist between bottom-up estimates, informed by ground-based flux measurements, and top-down estimates derived from spaceborne total column CH_4. Despite the extensive coverage of satellite CH_4 concentration observations, challenges remain with using top-down estimates to test bottom-up models, mainly because of the uncertainties in the satellite retrievals, the model representation errors, the variable prior emissions, and the confounding role of the posterior error covariance structures. Here, we use satellite-based top-down CH_4 flux estimates (2010–2012) to test and refine 42 bottom-up estimates of wetland emissions that use a range of hypothesized wetland extents and process controls. Our comparison between bottom-up models and satellite-based fluxes innovatively accounts for cross-correlations and spatial uncertainties typically found in top-down inverse estimates, such that only the information from satellite observations and the atmospheric transport model is kept as a constraint. We present a satellite-constrained wetland CH_4 ensemble product derived from assembling the highest-performance bottom-up models, which estimates global wetland CH_4 emissions of 148 (117–189, 5th–95th percentile) Tg CH_4 yr^{-1}. We find that tropical wetland emissions contribute 72% (63%–85%) to the global wetland total. We also find that a lower-than-expected temperature sensitivity agrees better with atmospheric CH_4 measurements. Overall, our approach demonstrates the potential for using satellites to quantitatively refine bottom-up wetland CH_4 emission estimates, their latitudinal distributions, and their sensitivity to climate.

Plain Language Summary Wetland methane (CH_4) emissions represent about 30% of the global CH_4 source and remain its most uncertain component. To test and refine bottom-up estimates of wetland emissions using satellite-informed top-down CH_4 fluxes, we present an approach that comprehensively accounts for prior flux assumptions, posterior cross-correlations, and spatial uncertainties in top-down flux estimates. Our results place new constraints on the latitudinal distribution of wetland emissions for bottom-up estimates: We find that tropical wetland emissions contribute 72% (63%–85%) to the global wetland total. We also find that for bottom-up model estimates, a lower-than-expected temperature sensitivity agrees better with atmospheric CH_4 measurements. Overall, our approach demonstrates the potential for using satellite-inferred CH_4 flux estimates to quantitatively refine bottom-up estimates and their sensitivity to climate.

1. Introduction

Methane (CH_4) has 28 times the global warming potential of CO_2 on a 100-year time scale (Myhre et al., 2013). Atmospheric CH_4 concentrations have increased by more than 150% since the pre-industrial age, and are

Author Contributions:
Conceptualization: John R. Worden, A. Anthony Bloom, Daniel J. Jacob
Data curation: A. Anthony Bloom, Yuzhong Zhang, Benjamin Poulter, Daniel J. Jacob
Formal analysis: A. Anthony Bloom
Funding acquisition: John R. Worden, A. Anthony Bloom
Investigation: John R. Worden, A. Anthony Bloom, Benjamin Poulter, Yi Yin, Sudhanshu Pandey, Joannes D. Maasakkers, Xiao Lu, Lu Shen, Jianxiong Sheng, Christian Frankenberg, Charles E. Miller
Methodology: John R. Worden, A. Anthony Bloom, Yuzhong Zhang, Daniel H. Cusworth, Yi Yin, Daniel J. Jacob
Project Administration: John R. Worden, A. Anthony Bloom
Resources: John R. Worden, A. Anthony Bloom, Yuzhong Zhang, Benjamin Poulter, Daniel H. Cusworth, Yi Yin, Xiao Lu, Lu Shen, Jianxiong Sheng, Christian Frankenberg, Charles E. Miller, Daniel J. Jacob
Supervision: John R. Worden, A. Anthony Bloom, Daniel J. Jacob
Validation: John R. Worden, A. Anthony Bloom, Daniel H. Cusworth, Joannes D. Maasakkers, Jianxiong Sheng
Visualization: A. Anthony Bloom
Writing – original draft: John R. Worden, A. Anthony Bloom, Yuzhong Zhang, Benjamin Poulter, Daniel H. Cusworth, Yi Yin, Sudhanshu Pandey, Joannes D. Maasakkers, Xiao Lu, Lu Shen, Jianxiong Sheng, Christian Frankenberg, Charles E. Miller, Daniel J. Jacob
Writing – review & editing: John R. Worden, A. Anthony Bloom, Benjamin Poulter, Daniel H. Cusworth, Yi Yin, Sudhanshu Pandey, Joannes D. Maasakkers, Xiao Lu, Lu Shen, Jianxiong Sheng, Christian Frankenberg, Charles E. Miller, Daniel J. Jacob

directly responsible for approximately 20% of the anthropogenic radiative forcing (IPCC, 2013; Kirschke et al., 2013). Wetland CH_4 emissions represent about 30% of the total CH_4 source, and remain the most uncertain component of the atmospheric CH_4 budget (Saunois et al., 2020a). The global wetland CH_4 budget differs substantially within and between top-down and bottom-up approaches. For example, bottom-up modeling estimates range from 117 to 203 Tg CH_4 yr^{-1} and top-down atmospheric inversion estimates range from 111 to 167 Tg CH_4 yr^{-1} from wetlands (Tian et al., 2016). The largest uncertainties in bottom-up modeling approaches stem from wetland inundation extent (driver data), biogeochemical process description (model structure), and responses to climatic variability (parameter uncertainty) (Bloom et al., 2017a; Melton et al., 2013; Pandey et al., 2020; Poulter et al., 2017; Wania et al., 2013; Zhang et al., 2018). For top-down inversions, the uncertainties are due to concentration data retrieval, atmospheric chemistry, model errors related to atmospheric transport, and bottom-up information in the distribution of emissions (Maasakkers et al., 2021). Reconciling bottom-up and top-down emissions estimates is key to understanding the spatio-temporal distribution of wetland CH_4 fluxes and reducing uncertainty on global CH_4-climate feedbacks in the coming decades.

Atmospheric inversions use observations of atmospheric column CH_4 to provide a constraint on the global scale spatial and temporal variability of wetland CH_4 emissions (Lu et al., 2021; Turner et al., 2019; Zhang et al., 2021). Attempts have been made to evaluate the performance of bottom-up models with CH_4 flux estimates from atmospheric inversions (Hayman et al., 2014; Spahni et al., 2011). However, top-down inversion results can be difficult to compare directly to bottom-up models because of their inherent uncertainty from model transport and chemistry, a coarser spatial resolution, and absence of process-level emission controls (e.g., soil C decomposition and water table). Atmospheric inversion solutions at specific locations are often correlated spatially with solutions in other regions, due to limited observational constraints. When observational constraints are relatively weak—For example, due to atmospheric transport patterns or limited observational coverage—the inversion solution depends strongly on the prior CH_4 flux estimates. As a result, much of the interpretation of emissions processes is confounded by prior CH_4 flux assumptions that are required to constrain the atmospheric inversion solution.

Here, we employ a Bayesian methodology to evaluate the skill of a range of bottom-up biogeochemical wetland CH_4 models that incorporate different biogeochemical structures, wetland extent, and parametrizations by comparing them to satellite-based atmospheric inversion estimates of wetland CH_4 emissions. Our study does not produce top-down or bottom-up estimates, but makes the two comparable by accurately accounting for the error characteristics of the inversion estimates, namely the limited spatial resolution, cross-correlations, and random uncertainties in top-down atmospheric inversions estimates (Section 2.3). We then compare common process-level drivers among models to assess which climatic drivers best explain the spatial and temporal variability of wetland CH_4 emissions (Section 2.4). The Bayesian evaluation of bottom-up models with top-down inversions allows us to reduce the large uncertainty on estimates of the distribution and temperature sensitivity of wetland CH_4 emissions. We summarize the datasets used in this methodology and the steps for testing and updating wetland biogeochemistry models with top-down measurements in Figure 1.

2. Data and Methods

2.1. Inverse Analysis of GOSAT Observations

Atmospheric CH_4 inverse problems estimate fluxes on a geospatial grid using observed concentrations of CH_4. The TANSO-FTS instrument onboard the Greenhouse Gases Observing Satellite (GOSAT; Kuze et al., 2009) provides global column-averaged dry mixing ratios of CH_4 (XCH_4; Parker et al., 2020). These observations are related to fluxes through an atmospheric transport and chemistry model. The posterior wetland CH_4 emission in our analysis is from a global flux inversion using GOSAT observations from 2010–2018 (Zhang et al., 2021). In addition to wetland emissions (resolved at 14 subcontinental regions and for individual months), the inversion by Zhang et al. (2021) also simultaneously optimizes anthropogenic CH_4 emissions (2010–2018 mean and trend on a 4° × 5° grid) and tropospheric OH concentration (the main sink of CH_4, hemispheric averages estimated annually) (Zhang et al., 2021). The inversion used WetCHARTs v1.0 Extended Ensemble (2010–2018) (Bloom et al., 2017b) as the prior estimates for wetland emissions (Zhang

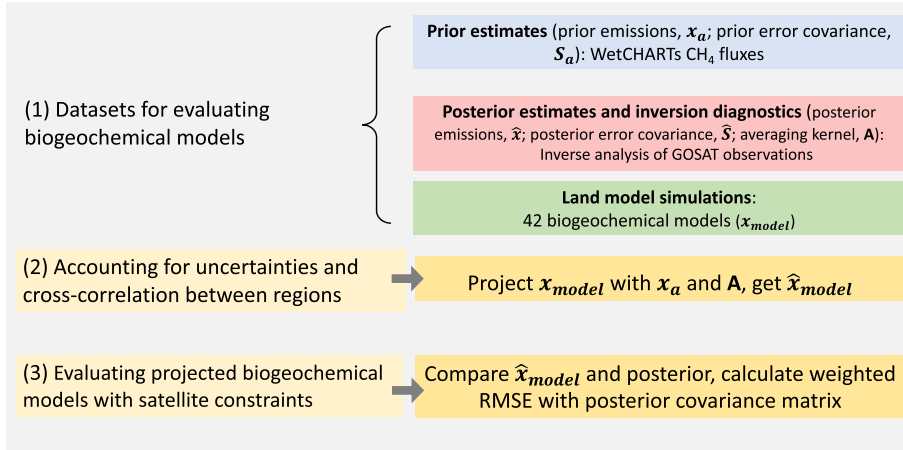

Figure 1. The workflow for constraining biogeochemical models with top-down (atmospheric inversion) CH_4 flux estimates. Datasets for our Bayesian methodology include (1) the prior estimates (WetCHARTs CH_4 emissions); (2) the posterior estimates and inversion diagnostics that allow for an explicit correction for the impact of the prior data; and (3) 42 biogeochemical land model simulations.

et al., 2021). For more details on the atmospheric inversion, readers are referred to Zhang et al. (2021) and a discussion on the quasi-linearity of the inverse problem can be found in Text S2.

The Zhang et al. (2021) global flux inversion analytically solves the inverse problem assuming Gaussian errors with a Bayesian optimal estimation (OE) approach (Maasakkers et al., 2019, 2021). A feature of this inversion approach is that it provides an averaging kernel matrix (**A**) and a posterior error covariance matrix ($\hat{\boldsymbol{S}}$) for the posterior estimates ($\hat{\boldsymbol{x}}$) of wetland emissions. The posterior covariance for the wetlands automatically includes the cross-state error from the other emission sectors and therefore they are accounted for in our error analysis (Worden et al., 2004). These inversion diagnostics allow for an explicit representation of the impact of the prior estimates (including spatial uncertainties and cross-correlations) for the inversion-based estimates of wetland CH_4 emissions (Rodgers, 2000). In the Appendix (Supporting Information), we demonstrate in detail why we need to account for uncertainties and cross-correlations before using inversion results to constrain land models (Equations A1-A3 in the Supporting Information) and show how elements in **A** relate to uncertainties and cross-correlations of regional CH_4 emissions (Figure S4). In Section 2.3, we introduce the approach to account for the prior estimates and spatial resolution with diagnostic quantities from the Bayesian inversion.

2.2. Biogeochemical Bottom-Up Models

We evaluated 42 global wetland biogeochemical model simulated emissions with the satellite-based inversion product. These bottom-up models represent the state-of-the-science ability to simulate large-scale wetland CH_4 emissions, which cover different biogeochemical structures, wetland extent, and parametrizations, including 18 members from WetCHARTs v1.3.1 Extended Ensembles (2001–2019; Bloom et al., 2017b), 11 members from Global Carbon Project version 1 (GCPv1, 2000–2012; Poulter et al., 2017; Saunois et al., 2016), and 13 members from GCPv2 (2000–2017; Saunois et al., 2020b). Both GCP versions are chosen because they are driven by different wetland extent maps with different spatiotemporal variabilities. We use only the 2010–2012 data for comparison because GCPv1 simulations end in 2012. To examine the effect of using only a 3-year overlap period in scoring model performance, a longer period ranking (2010–2017) is done with WetCHARTs and GCPv2. We discuss the effect of using different periods on evaluating model performance in Section 3.1.

WetCHARTs is a process-informed wetland CH_4 emission data set for atmospheric chemistry and transport modeling, representing a probability distribution of biogeochemical process control uncertainties (Bloom et al., 2017a). The WetCHARTs Extended Ensemble (EE) was derived by combining a range of CH_4:C temperature sensitivities (Q_{10} CH_4:C), three global wetland emissions scaling factors, and two dynamic wetland

extent maps. Q_{10} CH_4:C is the relative CH_4: C respiration for a 10°C increase. A Q_{10} CH_4:C value equal 1 thus indicates CH_4 respiration is as sensitive to the temperature as heterotrophic CO_2 respiration. In different WETCHARTs configurations, Q_{10} CH_4:C equal 1, 2, and 3 to represent low, medium, and high temperature sensitivity of CH_4 emissions. Any value smaller than 1 is not considered since the temperature sensitivity of CH_4 emissions is higher than CO_2 respiration across ecosystem scales (Yvon-Durocher et al., 2014). The global wetland emissions in WetCHARTs models are calibrated with global emission scaling factors so that for each model the total emission in 2009–2010 amounts to 124.5, 166, and 207.5 Tg CH_4 yr^{-1} based on the uncertainty range of top-down wetland CH_4 emission estimates (Saunois et al., 2016). Two wetland extent inventories are used to represent wetland extent fraction at 0.5 by 0.5° resolution, including GLOBCOVER (Bontemps et al., 2011) and Global Lakes and Wetlands Database (GLWD, Lehner & Döll, 2004). GLOBCOVER is a global land-cover map using the fine resolution (300 m) mode data from the MERIS sensor onboard ENVISAT satellite. GLWD is an inventory-based product that synthesizes a number of best available sources for lakes and wetlands on a global scale. Monthly ERA-Interim precipitation is used to represent the seasonal variation in hydrology. Hereafter, we use WC_GLOBCOVER_PREC and WC_GLWD_PREC to refer to the two wetland extent datasets. This approach empirically provides first-order constraints on the role of carbon, water and temperature on the spatiotemporal variability of wetland CH_4 emissions, and indirectly accounts for the individual processes of production, oxidation, and transport pathways from belowground to the atmosphere. Variants of this formulation have been used within a range of wetland CH_4 emission models (e.g., Bloom et al., 2012; Melton et al., 2013; Zhang et al., 2017).

GCP models are land biosphere models: their CH_4 modules represent various formulations of model structure, parameterization, and initialization (Poulter et al., 2017; Saunois et al., 2020b). The models were simulated following a common protocol for model spin-up and transient runs, using standardized climate and atmospheric CO_2. Wetland inventories are used to set the long-term annual mean wetland area, and seasonal cycles are added from fractional surface water using data from the Surface Water Microwave Product Series (SWAMPS). GCPv1 uses GLWD (Global Lakes and Wetlands Data Set; Lehner & Döll, 2004) coupled with SWAMPSv2 (Schroeder et al., 2015), for clarity in this paper we refer it as GCPv1_GLWD_SWAMP. GCPv2 uses various regional inventory datasets (Gumbricht et al., 2017; Hugelius et al., 2014; Widhalm et al., 2015) coupled with SWAMPS v3.2 (Jensen & Mcdonald, 2019), hereafter GCPv2_Mix_SWAMP.

One of the improvements in GCPv2 is decreased high-latitude emissions due to decreased wetland area after correction for the "double counting" of wetland extent (Saunois et al., 2020a). We use our approach here to see if the GCPv2 model simulations better agree with satellite observations than GCPv1. CH_4 emissions from rice paddies are excluded in both WetCHARTs and GCP simulations. WetCHARTs implicitly includes emission from non-wetland freshwater bodies. GCPv1 and v2 exclude non-wetland freshwater based on satellite observations. We discuss the different ways of treating non-wetland freshwater and its potential impact on our analysis in Section 3.5. More details on model simulations and wetland extent can be found in Bloom et al. (2017a), Poulter et al. (2017), and Saunois et al. (2020a).

2.3. Accounting for the Prior Estimates and Spatial Resolution

The comparison between a gridded inverse solution and an independent wetland model is complicated by the fact that the inverse solution contains cross-correlated information (Worden et al., 2004) and corresponding varying spatial resolution, as discussed in Section 2.1 and the Appendix (Supporting Information). Therefore, for an appropriate comparison between model and estimate, a wetland model needs to be projected through an observation operator first (Rodgers, 2000). This takes the form of the following:

$$\hat{\boldsymbol{x}}_{\mathbf{model}} = \boldsymbol{x}_a + A\left(\boldsymbol{x}_{\mathbf{model}} - \boldsymbol{x}_a\right) \quad (1)$$

where $\hat{\boldsymbol{x}}_{\mathbf{model}}$ is projected model emissions, $\boldsymbol{x}_{\mathbf{model}}$ is the estimated CH_4 emission from the biogeochemical model of interest, and $\boldsymbol{x}_a$ is the prior estimates used in inversion. **A** is averaging kernel matrix, the diagonal terms in **A** describe the sensitivity of inversion results to the variability of the "true" emissions, and the cross-terms describe the sensitivity of the wetland estimate to emissions from other regions. The calculation of **A** requires the prior and posterior covariance matrix, as described by Zhang et al. (2021) and Rodgers (2000). The approach here allows the modeled estimates ($\boldsymbol{x}_{\mathbf{model}}$) to be "viewed" in a consistent way ($\hat{\boldsymbol{x}}_{\mathrm{model}}$) with the inversion and essentially removes the impact of the prior estimates. Figure S1 shows the

difference before and after the projection of the model through Equation 1. The inversion-model mismatch is enlarged during the information-rich period and reduced for the poor signal period. We then compare these projected model emissions to posterior fluxes to rank bottom-up wetland models.

2.4. Evaluating Biogeochemistry Model Performance

We evaluate the weighted Root Mean Square Error (wRMSE) between projected biogeochemistry model emissions ($\hat{\boldsymbol{x}}_{\text{model}}$, see Section 2.3) and inversion-based estimates of wetland CH_4 emissions ($\hat{\boldsymbol{x}}$). Specifically, the wRMSE use the posterior covariance matrix ($\hat{\mathbf{S}}$) to account for spatial uncertainties and cross-correlations between regions from the inversion:

$$\text{wRMSE} = \left(\frac{\left(\hat{\boldsymbol{x}} - \hat{\boldsymbol{x}}_{\mathbf{model}}\right)\hat{\mathbf{S}}^{-1}\left(\hat{\boldsymbol{x}} - \hat{\boldsymbol{x}}_{\mathbf{model}}\right)^{\mathrm{T}}}{\boldsymbol{N}} \right) \tag{2}$$

where N is the number of elements in $\hat{\boldsymbol{x}}$. The wRMSE metric represents the overall model performance across the globe (14 regions by 36 monthly emissions). Based on the wRMSE ranking of each biogeochemical model, we group the top one-third as the "Highest-Performance model ensemble (HP)" and the bottom one-third as the "Lowest-Performance model ensemble (LP)".

To highlight the significance of removing the impact of the prior assumptions from atmospheric inversion estimates, we show the relative differences in model performance before and after accounting for cross-correlations and spatial uncertainties (Table S4).

To further assess whether satellite-based flux estimates provide insights on biogeochemical processes, we use the factorial WetCHARTs configurations to evaluate the relationships between key process configurations (temperature sensitivity of CH_4 production, global wetland emissions scaling factors, wetland extent maps), and corresponding model performance (wRMSE). For each process p, we calculate the marginal performance of each model m, $\Delta\text{wRMSE}_{(m,p)}$, as follows:

$$\Delta\text{wRMSE}_{(m,p)} = \text{wRMSE}_{(m)} - \text{wRMSE\_MM}_{(m,p)} \tag{3}$$

where $\text{wRMSE\_MM}_{(m,p)}$ is the reference mean wRMSE for all configurations of p for the reference model subset which share the same process configurations other than p (see Table S1). For example, for all three WetCHARTs models that use the same wetland extent map (GLOBCOVER) and global wetland CH_4 emissions scaling factor (124.5 Tg CH_4 yr^{-1}), their reference mean performance $\text{wRMSE\_MM}_{(m,p)}$ will be the average of all three wRMSE values, and their marginal performance $\Delta\text{wRMSE}_{(m,p)}$ will depend on their Q_{10} CH_4:C value (Q_{10} CH_4:C = 1, 2, or 3). Larger $\Delta wRMSE$ values indicate a better model agreement with atmospheric estimates (relative to the reference model subset).

3. Results and Discussion

3.1. Global, Latitudinal, Regional CH_4 Emission and Seasonal Variation

Median global CH_4 emissions (2010–2012) from the Highest-Performance model ensemble (HP) is 148 Tg CH_4 yr^{-1} (117–189, 5th–95th percentiles), about 25% lower than the median (201 Tg CH_4 yr^{-1}) of the Lowest-Performance model ensemble (LP) models (160–218, 5th–95th percentiles; Figure 2, Table 1). The global wetland emission from HP generally agrees with independent top-down estimates of 149–159 Tg CH_4 yr^{-1} (Ghosh et al., 2015) and 111–167 Tg CH_4 yr^{-1} (Tian et al., 2016), whereas LP exhibits higher values in general agreement in line with a range of bottom-up estimates of 141–264 Tg CH_4 yr^{-1} (Melton et al., 2013), 153–227 Tg CH_4 yr^{-1} (Saunois et al., 2016), and 160–206 Tg CH_4 yr^{-1} (Poulter et al., 2017).

The total tropical wetland emissions (south of 23°N) are similar between HP and LP ensembles (median values are 111 and 114 Tg CH_4 yr^{-1}, respectively), but with contrasting spatial distributions. Amazon wetland emissions account for the largest tropical emission source in both ensembles, albeit with lower emissions across HP models (median = 34, range = 17–42 Tg CH_4 yr^{-1}) relative to the LP ensemble (median = 40 Tg CH_4 yr^{-1}, range = 20–66 Tg CH_4 yr^{-1}) (Table S2). Across non-tropical wetlands (north of 23°N) LP emissions

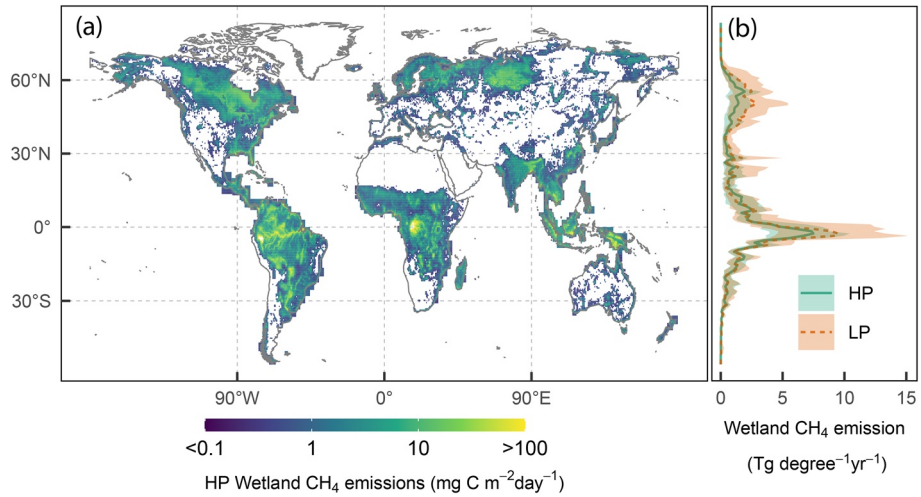

Figure 2. Mean wetland CH_4 emissions during 2010–2012 from the Highest-Performance (HP) model ensemble (a); Zonal profiles of wetland CH_4 emissions over 2010–2012 (b): Median of Lowest-Performance model ensemble (LP, brown dashed line) and 5th-95th percentile range (brown area); Median of HP (green solid line) and 5th-95th percentile range (green area).

are 1.5 times more than those of HP (64 and 43 Tg CH_4 yr^{-1}, respectively), where about two-thirds of excess CH_4 emissions from the LP ensemble are in high-latitude regions (Table 1). In particular, median emissions from Alaska, Boreal North America, and Temperate North America are larger by a factor of two in the LP ensemble. We found larger seasonal emissions rates in LP in all cold regions and two temperate regions in East Asia and North America, which is mainly due to larger seasonal amplitudes in LP model wetland extent dynamics (Figures S2, S3 and Table S2). Overall, HP models have a higher contribution from the tropics to the global budget (72%) than LP models (62%).

We find that HP model emissions are consistent with the annual and month-to-month seasonality of independent aircraft-based wetland CH_4 emission in the Alaska region (Carbon in Arctic Reservoirs Vulnerability Experiment, CARVE campaign) (Miller et al., 2016), where May-October 2012 emissions amount to 1.66 ± 0.95 and 1.80 ± 0.45 Tg CH_4, respectively. Although both HP and the CARVE all datasets have

Table 1
Wetland CH_4 Emissions (2010–2012) for the Globe, Non-tropics, Tropics, High-Latitude, and Temperate Regions, and the Relative Contribution of Each Region to Global Emissions

	Highest-performance model ensemble (HP)	Lowest-performance model ensemble (LP)	Prior estimates
	CH_4 emission (Tg C $year^{-1}$, 2010–2012)		
Globe	148.1 (116.5–189.0)	201.0 (160.7–217.8)	164.4 (122.6–206.8)
Non-tropics	42.7 (20.0–60.5)	63.5 (24.6–109.1)	37.4 (20.5–73.5)
Tropics	111.0 (71.1–139.3)	113.7 (90.6–172.7)	119.7 (82.8–171.2)
High-latitude	28.5 (12.4–41.4)	44.1 (13.6–79.0)	22.6 (11.7–55.2)
Temperate	12.8 (7.9–25.2)	20.5 (9.2–41.9)	12.4 (7.3–20.9)
	Latitudinal contribution to CH_4 emission		
Non-tropics/globe ratio	28% (15%–37%)	38% (13%–52%)	23% (13%–43%)
Tropics/globe ratio	72% (63%–85%)	62% (48%–87%)	77% (57%–87%)
High-latitude/globe ratio	17% (9%–27%)	26% (7%–36%)	14% (7%–32%)
Temperate/globe ratio	9% (6%–15%)	10% (5%–24%)	9% (6%–11%)

Note. The prior estimates represent the WetCHARTs models that were used as prior fluxes in the inversion. The values represent median and the 5th–95th percentile ranges are shown in the brackets.

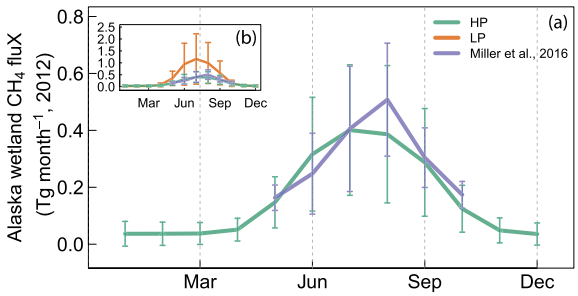

Figure 3. Evaluation of the satellite-informed highest-performance (HP) and lowest-performance (LP) ensembles against independent aircraft-based (CARVE; Miller et al., 2016) estimates of wetland emissions over the Alaska region. Error bars represent one standard deviation.

notable uncertainties (Figure 3a), LP emissions and uncertainties during the same period (4.2 ± 3.7 Tg CH_4) substantially exceed the CARVE and HP emission estimates (Figure 3b).

3.2. Atmospheric CH_4 Constraints on Land Model Processes

We compare the parameter values and wetland extent maps against the model performance (wRMSE) within the WetCHARTs members (Figure 4) and find that (a) models using a Q_{10} CH_4:C equals 1 have significantly higher performance than the ones using larger Q_{10} CH_4:C values; (b) models with the smallest global wetland CH_4 emission scaling factor perform better than those with larger scaling factors; and (c) models using the GLOBCOVER derived wetland extent maps outperform those using the GLWD map. Relative to the median WetCHARTs configurations, atmospheric constraints indicate a low temperature sensitivity and a low mean global wetland emissions scaling factor, and satellite-based wetland extent (GLOBCOVER) generally leads to better agreement with atmospheric CH_4 measurements.

Despite the lack of parameter information from GCP models, we find most GCPv2 simulations perform better than GCPv1 (Table S1). Since 10 out of 11 GCPv1 land-surface models also participated in GCPv2 (13 models), we compared their performance and find the same land surface models agree better with satellite CH_4 observation when using a Mix_SWAMP extent map rather than GLWD_SWAMP (e.g., TRIPLEX-GHG). Of all the land models compared, a majority of low-ranked simulations use a GLWD-based annual extent map (9 out of 14), and most high-ranked simulations use a non-GLWD-based map (10 out of 14).

In both GCP v1 and GCP v2 simulations, LPX-Bern (Land surface Processes and eXchanges model of the University of Bern; (Spahni et al., 2013)) and JULES (the Joint UK Land Earth Simulator; Hayman et al., 2014) have the best agreement with satellite data (Table S1). This may be due to their more realistic model structures or better choice of parameter values in representing the seasonality of CH_4 emissions, which awaits further investigation.

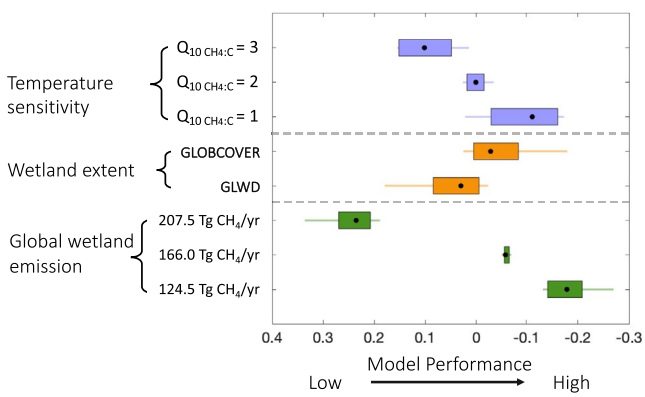

Figure 4. Marginal weighted weighted Root Mean Square Error (wRMSE) performance (see Section 2.4) of the factorial WetCHARTs model ensemble, with respect to individual temperature sensitivity of CH_4:C emissions (Q_{10} CH_4:C), global wetland emission scaling factors, and wetland extent datasets. The black dots represent medians, boxes represent the 25th–75th percentile ranges, and lines represent 5th–95th percentile ranges. Negative values on the *x* axis indicate the wRMSE of a model is smaller than the reference mean, and thus the model has a better performance than the average.

3.3. Sensitivity of CH_4 to Climatic, Physical, and Biological Drivers

We find wetland extent and precipitation have the highest correlation with CH_4 emission over tropical regions in both HP and LP (Figure S6). This finding is in line with previous studies that find declining wetland area to be the dominant control of decreased tropical CH_4 emissions over 1993–2004 (Papa et al., 2010; Poulter et al., 2017), and that rain-fed pulses of CH_4 from East Africa in 2018–2019 contribute to the atmospheric growth rate (Lunt et al., 2021). Much lower correlations between temperature/carbon (C) availability and CH_4 emissions are found in both the HP (0.31 and 0.13) and LP (0.29 and 0.28) ensembles in tropical regions, which implies that temperature and C availability are not the limiting factors in tropical wetland CH_4 emission (C availability is represented by heterotrophic respiration rate in biogeochemical models, data only available for WetCHARTs simulations).

In contrast to the tropics, non-tropical wetland CH_4 emissions exhibit a higher correlation with C availability and temperature in all models (Figure S6, 0.93 and 0.90 in HP, 0.91 and 0.88 in LP), followed by wetland extent and precipitation (0.75 and 0.79 in HP, 0.75 and 0.76 in LP). Our results indicate that C availability and temperature are highly correlated with CH_4 emissions in high-latitude and temperate regions, consistent

with previous studies that found temperature and decomposing substrate supply to be the dominant controls on non-tropical wetland CH_4 emissions (Chen et al., 2015; Ma et al., 2017; Schuur et al., 2015; Yvon-Durocher et al., 2014).

3.4. Implications for the Global and Regional CH_4 Budget

Altogether, we find that low global total emissions, a low temperature sensitivity, and satellite-based wetland extent are the primary factors driving biogeochemical model performance against the global inverse flux estimates (Figures 2b and 4). In addition, the highest-performance models estimate a higher fraction of CH_4 emissions from the tropics (72%) than the process-based modeling results of 66% (Melton et al., 2013), 55% (Bloom et al., 2010), and 48% from GCPv1 (Poulter et al., 2017), and the inverse modeling results of 63% (Bousquet et al., 2011), but are comparable to 76% from WetCHARTs v1 extended ensemble (Bloom et al., 2017a) and 74% from GCPv2 (Saunois et al., 2020a). Our results, therefore, imply a larger role of tropical CH_4 emissions in the global wetland emission budget.

The large uncertainties in predicting wetland CH_4 emission come from (a) climate and wetland extent predictions (drivers) (Andresen et al., 2020; Zhang et al., 2017); (b) process controls (model structures); and (c) climatic sensitivities of CH_4 productions (parameter values) (Poulter et al., 2017; Riley et al., 2011). Our approach enables the evaluation of terrestrial biosphere models with satellite-informed estimates and places constraints for land model predictions by telling which wetland extent maps, biogeochemical processes, and parameters values used in the models are more realistic, as discussed in Section 3.2 (Cox et al., 2013; Wenzel et al., 2016).

The high correlation to precipitation and wetland extent in both HP and LP models indicates increasing CH_4 emission in response to climate change, as wet areas in the tropics are likely to get wetter, have increased anoxic soil area, and become saturated for longer periods (Chou et al., 2009; Neelin et al., 2003). In line with our findings, shifting precipitation patterns have been found to drive long-term simulated CH_4 emission changes in the tropics (Zhang et al., 2017). Our analysis reveals how wetlands across the globe respond to variations in temperature, precipitation, inundation, and carbon availability. However, with 3 years of data (2010–2012), we cannot refute the possibility that, on decadal-centennial timescales, temperature is the primary control on tropical wetland emissions. With longer-term results, our analysis can be used as constraints on terrestrial biosphere model CH_4 simulations.

A poor understanding of tropical wetland biogeochemistry and associated spatial heterogeneity lead to large inter-model discrepancies in tropical wetland CH_4 emissions (Poulter et al., 2017; Riley et al., 2011). The lack of ground-based CH_4 emission observations (Bridgham et al., 2013; Melton et al., 2013) further limits the evaluation of process-based model performance in the tropics. Satellite-based observations with improved accuracy and finer spatiotemporal resolutions, such as TROPOMI and GeoCarb, are expected to offer additional information for process-based model validation, especially for data-scarce regions (Bloom et al., 2016). With our Bayesian methodology, we showcase the large differences in model performance before and after considering cross-correlations and spatial uncertainties, emphasizing the importance of removing the prior error from atmospheric inversion estimates (Table S4). Our findings, and approach for accounting for these correlations, prior estimates, and spatial resolutions, show how space-borne measurements of total column CH_4 can evaluate and ultimately place constraints on global wetland biogeochemistry.

4. Remaining Uncertainties, Future Directions, and Summary

While our estimates account for the spatial resolution and error associated with the inversion of observations to fluxes, we do not explicitly account for errors in model transport and chemistry, such as interhemispheric mixing time, vertical mixing, tropopause height, and stratospheric gradient. These errors are important and can be accounted for if the corresponding posterior covariance is provided, possibly through multi-model comparisons (e.g., Schuh et al., 2019) or by integrating measurements with different sensitivities to the profile of CH_4 (e.g., Jiang et al., 2013, 2017). We thus advocate studies that either characterize or mitigate these errors to offer better constraints for bottom-up estimates. We note that the methodology presented in this study can only apply to atmospheric CH_4 inversions that calculate prior and posterior covariances (Turner et al., 2015). The methodology can also be applied to other inversion methods (e.g.,

4D-Var methods) if these can approximate posterior covariance estimates (Chevallier et al., 2007, 2010; Liu et al., 2014; Yin et al., 2020). In a 4D-Var system, the posterior flux uncertainty is often approximated using a Monte Carlo approach (Chevallier et al., 2007; Liu et al., 2014). In a Monte Carlo approach, an ensemble of prior states and observations accounting for the prior and observation gaussian error statistics are generated, and the standard deviation of the ensemble posterior fluxes gives the estimates of posterior flux uncertainty. In this way, the averaging matrix could be approximated using the same method as the analytical solution, provided that the posterior covariance matrix is available.

Non-wetland freshwater bodies (lakes, rivers, and ponds) are potentially a significant CH_4 source and have relative uncertainties larger than that of wetland fluxes (Bridgham et al., 2013; Saunois et al., 2020a). WetCHARTs includes emissions from non-wetland freshwater bodies and WetCHARTS is used as the prior for the GEOS-Chem inversion so that we expect the corresponding flux estimates to include their effects in the inversion. GCPv1 excludes permanent water bodies, rivers, snow, and ice with satellite-based Land-cover data MOD12Q1 V004 (Friedl et al., 2010). GCPv2 removes permanent non-wetland freshwater using the Global Surface Water data set (Pekel et al., 2016), with the assumed criteria that permanent waters are present for more than half of the 32-year observing period. Quantitatively differentiating wetland and non-wetland emissions is therefore important but challenging due to the current spatiotemporal resolution of data on surface inundation (Pekel et al., 2016; Schroeder et al., 2015). Our results indicate that aquatic emissions are much lower than those recently reported using bottom-up methods (Rosentreter et al., 2021; Saunois et al., 2020a) highlighting an important topic that needs reconciling by the scientific community.

Overall, our approach provides a quantitative and comprehensive means to test global-scale biogeochemical models using satellite CH_4 measurements—And associated hypotheses relating to CH_4 emissions—thereby providing a much-needed constraint on the uncertain role of wetlands in the global atmospheric CH_4 budget.

Conflict of Interest

The authors declare that they have no conflict of interest.

Data Availability Statement

The data set for the 2010–2012 posterior wetland fluxes and the averaging kernel of the transport model is available at an open-access repository (https://doi.org/10.5281/zenodo.4052518; Zhang et al., 2021). The WetCHARTs v1.0 is available at the Oak Ridge National Laboratory Distributed Active Archive Center (ORNL DAAC, https://daac.ornl.gov/CMS/guides/CMS_Global_Monthly_Wetland_CH4.html). The WetCHARTs v1.3.1 is available at the ORNL DAAC, https://doi.org/10.3334/ORNLDAAC/1915. ERA-Interim temperature and precipitation datasets were obtained from http://apps.ecmwf.int/datasets/data/interim-full-mnth. CARDAMOM 2001–2010 heterotrophic respiration outputs are available at http://datashare.is.ed.ac.uk/handle/10283/875; Global Carbon Project v1 and v2 are available at https://doi.org/10.18160/GCP-CH4-2019 and from the Global Carbon Project (https://www.globalcarbonproject.org/methanebudget/).

Acknowledgments
Part of this research was carried out at the Jet Propulsion Laboratory, California Institute of Technology, under a contract with the National Aeronautics and Space Administration. Funding for this study was provided through the NASA Carbon Monitoring System (CMS) grant (#NNH14ZDA001N-CMS), NASA CMS (#NNH18ZDA001N-CMS). Y. Zhang acknowledges funding by NSFC (Project 42007198) and Westlake University.

References

Andresen, C. G., Lawrence, D. M., Wilson, C. J., David McGuire, A., Koven, C., Schaefer, K., et al. (2020). Soil moisture and hydrology projections of the permafrost region-a model intercomparison. *The Cryosphere*, *14*(2), 445–459. https://doi.org/10.5194/tc-14-445-2020

Bloom, A. A., Bowman, K., Lee, M., Turner, A. J., Schroeder, R., Worden, J. R., et al. (2017b). *CMS: Global 0.5-deg wetland methane emissions and uncertainty (WetCHARTs v1.0)*. Oak Ridge, Tennessee, USA: ORNL DAAC. https://doi.org/10.3334/ORNLDAAC/1502

Bloom, A. A., Bowman, W. K., Lee, M., Turner, J. A., Schroeder, R., Worden, R. J., et al. (2017a). A global wetland methane emissions and uncertainty dataset for atmospheric chemical transport models (WetCHARTs version 1.0). *Geoscientific Model Development*, *10*(6), 2141–2156. https://doi.org/10.5194/gmd-10-2141-2017

Bloom, A. A., Lauvaux, T., Worden, J., Yadav, V., Duren, R., Sander, S. P., & Schimel, D. S. (2016). What are the greenhouse gas observing system requirements for reducing fundamental biogeochemical process uncertainty? Amazon wetland CH_4 emissions as a case study. *Atmospheric Chemistry and Physics*, *16*(23), 15199–15218. https://doi.org/10.5194/acp-16-15199-2016

Bloom, A. A., Palmer, P. I., Fraser, A., & Reay, D. S. (2012). Seasonal variability of tropical wetland CH_4 emissions: The role of the methanogen-available carbon pool. *Biogeosciences*, *9*, 2821–2830. https://doi.org/10.5194/bg-9-2821-2012

Bloom, A. A., Palmer, P. I., Fraser, A., Reay, D. S., & Frankenberg, C. (2010). Large-scale controls of methanogenesis inferred from methane and gravity spaceborne data. *Science*, *327*(5963), 322–325. https://doi.org/10.1126/science.1175176

Bontemps, S., Defourny, P., Van Bogaert, E., Arino, O., Kalogirou, V., & Perez, J. R. (2011). *GLOBCOVER 2009 products description and validation report*, (Vol. 2). Retreived from https://epic.awi.de/id/eprint/31014/16/GLOBCOVER2009_Validation_Report_2-2.pdf

Bousquet, P., Ringeval, B., Pison, I., Dlugokencky, E. J., Brunke, E.-G., Carouge, C., et al. (2011). Source attribution of the changes in atmospheric methane for 2006–2008. *Atmospheric Chemistry and Physics*, *11*(8), 3689–3700. https://doi.org/10.5194/acp-11-3689-2011

Bridgham, S. D., Cadillo-Quiroz, H., Keller, J. K., & Zhuang, Q. (2013). Methane emissions from wetlands: Biogeochemical, microbial, and modeling perspectives from local to global scales. *Global Change Biology*, *19*(5), 1325–1346. https://doi.org/10.1111/gcb.12131

Chen, X., Bohn, T. J., & Lettenmaier, D. P. (2015). Model estimates of climate controls on pan-Arctic wetland methane emissions. *Biogeosciences*, *12*(21), 6259–6277. https://doi.org/10.5194/bg-12-6259-2015

Chevallier, F., Bréon, F.-M., & Rayner, P. J. (2007). Contribution of the Orbiting Carbon Observatory to the estimation of CO_2 sources and sinks: Theoretical study in a variational data assimilation framework. *Journal of Geophysical Research Atmosphere*, *112*, D09307. https://doi.org/10.1029/2006JD007375

Chevallier, F., Ciais, P., Conway, T. J., Aalto, T., Anderson, B. E., Bousquet, P., et al. (2010). CO_2 surface fluxes at grid point scale estimated from a global 21 year reanalysis of atmospheric measurements. *Journal of Geophysical Research Atmospheres*, *115*(21), 1–17. https://doi.org/10.1029/2010JD013887

Chou, C., Neelin, J. D., Chen, C. A., & Tu, J. Y. (2009). Evaluating the "rich-get-richer" mechanism in tropical precipitation change under global warming. *Journal of Climate*, *22*(8), 1982–2005. https://doi.org/10.1175/2008JCLI2471.1

Cox, P. M., Pearson, D., Booth, B. B., Friedlingstein, P., Huntingford, C., Jones, C. D., & Luke, C. M. (2013). Sensitivity of tropical carbon to climate change constrained by carbon dioxide variability. *Nature*, *494*(7437), 341–344. https://doi.org/10.1038/nature11882

Friedl, M. A., Tan, B., Sulla-Menashe, A., Ramankutty, N., Sibley, A., Huang, X., & Huang, X. (2010). MODIS collection 5 global land cover: Algorithm refinements and characterization of new datasets. *Remote Sensing of Environment*, *114*(1), 168–182. https://doi.org/10.1016/j.rse.2009.08.016

Ghosh, A., Patra, P. K., Ishijima, K., Umezawa, T., Ito, A., Etheridge, D. M., et al. (2015). Variations in global methane sources and sinks during 1910–2010. *Atmospheric Chemistry and Physics*, *15*(5), 2595–2612. https://doi.org/10.5194/acp-15-2595-2015

Gumbricht, T., Roman-Cuesta, R. M., Verchot, L., Herold, M., Wittmann, F., Householder, E., et al. (2017). An expert system model for mapping tropical wetlands and peatlands reveals South America as the largest contributor. *Global Change Biology*, *23*(9), 3581–3599. https://doi.org/10.1111/gcb.13689

Hayman, G. D., O'Connor, F. M., Dalvi, M., Clark, D. B., Gedney, N., Huntingford, C., et al. (2014). Comparison of the HadGEM2 climate-chemistry model against in situ and SCIAMACHY atmospheric methane data. *Atmospheric Chemistry and Physics*, *14*(23), 13257–13280. https://doi.org/10.5194/acp-14-13257-2014

Hugelius, G., Strauss, J., Zubrzycki, S., Harden, J. W., Schuur, E. A. G., Ping, C. L., et al. (2014). Estimated stocks of circumpolar permafrost carbon with quantified uncertainty ranges and identified data gaps. *Biogeosciences*, *11*(23), 6573–6593. https://doi.org/10.5194/bg-11-6573-2014

IPCC. (2013). *Climate change 2013: The physical science basis contribution of working group I to the fifth assessment report of the intergovernmental panel on climate change*. Cambridge: Cambridge University Press.

Jensen, K., & Mcdonald, K. (2019). Surface water microwave product series version 3: A near-real time and 25-year historical global inundated area fraction time series from active and passive microwave remote sensing. *IEEE Geoscience and Remote Sensing Letters*, *16*(9), 1402–1406. https://doi.org/10.1109/lgrs.2019.2898779

Jiang, Z., Jones, D. B. A., Worden, H. M., Deeter, M. N., Henze, D. K., Worden, J., et al. (2013). Impact of model errors in convective transport on CO source estimates inferred from MOPITT CO retrievals. *Journal of Geophysical Research Atmospheres*, *118*(4), 2073–2083. https://doi.org/10.1002/jgrd.50216

Jiang, Z., Worden, J. R., Worden, H., Deeter, M., Jones, D. B. A., Arellano, A. F., & Henze, D. K. (2017). A 15-year record of CO emissions constrained by MOPITT CO observations. *Atmospheric Chemistry and Physics*, *17*(7), 4565–4583. https://doi.org/10.5194/acp-17-4565-2017

Kirschke, S., Bousquet, P., Ciais, P., Saunois, M., Canadell, J. G., Dlugokencky, E. J., et al. (2013). Three decades of global methane sources and sinks. *Nature Geoscience*, *6*(10), 813–823. https://doi.org/10.1038/ngeo1955

Kuze, A., Suto, H., Nakajima, M., & Hamazaki, T. (2009). Thermal and near infrared sensor for carbon observation fourier-transform spectrometer on the greenhouse gases observing satellite for greenhouse gases monitoring. *Applied Optics*, *48*(35), 6716–6733. https://doi.org/10.1364/AO.48.006716

Lehner, B., & Döll, P. (2004). Development and validation of a global database of lakes, reservoirs and wetlands. *Journal of Hydrology*, *296*(1), 1–22. https://doi.org/10.1016/j.jhydrol.2004.03.028

Liu, J., Bowman, K. W., Lee, M., Henze, D. K., Bousserez, N., Brix, H., et al. (2014). Carbon monitoring system flux estimation and attribution: Impact of ACOS-GOSAT XCO2 sampling on the inference of terrestrial biospheric sources and sinks. *Tellus Series B Chemical and Physical Meteorology*, *66*(1), 22486. https://doi.org/10.3402/tellusb.v66.22486

Lu, X., Jacob, D. J., Zhang, Y., Maasakkers, J. D., Sulprizio, M. P., Shen, L., et al. (2021). Global methane budget and trend, 2010-2017: Complementarity of inverse analyses using in situ (globalviewplus obspack) and satellite (gosat) observations. *Atmospheric Chemistry and Physics*, *21*(6), 4637–4657. https://doi.org/10.5194/acp-21-4637-2021

Lunt, M. F., Palmer, P. I., Lorente, A., Borsdorff, T., Landgraf, J., Parker, R. J., & Boesch, H. (2021). Rain-fed pulses of methane from East Africa during 2018–2019 contributed to atmospheric growth rate. *Environmental Research Letters*, *16*, 024021. https://doi.org/10.1088/1748-9326/abd8fa

Ma, S., Jiang, J., Huang, Y., Shi, Z., Wilson, R. M., Ricciuto, D., et al. (2017). Data-constrained projections of methane fluxes in a Northern Minnesota Peatland in response to elevated CO_2 and warming. *Journal of Geophysical Research: Biogeosciences*, *122*(11), 2841–2861. https://doi.org/10.1002/2017jg003932

Maasakkers, J. D., Jacob, D. J., Sulprizio, M. P., Scarpelli, T. R., Nesser, H., Sheng, J., et al. (2021). 2010–2015 North American methane emissions, sectoral contributions, and trends: A high-resolution inversion of GOSAT observations of atmospheric methane. *Atmospheric Chemistry and Physics*, *21*(6), 4339–4356. https://doi.org/10.5194/acp-21-4339-2021

Maasakkers, J. D., Jacob, D. J., Sulprizio, M. P., Scarpelli, T. R., Nesser, H., Sheng, J.-X., et al. (2019). Global distribution of methane emissions, emission trends, and OH concentrations and trends inferred from an inversion of GOSAT satellite data for 2010–2015. *Atmospheric Chemistry and Physics*, *19*, 7859–7881. https://doi.org/10.5194/acp-19-7859-2019

Melton, J. R., Wania, R., Hodson, E. L., Poulter, B., Ringeval, B., Spahni, R., et al. (2013). Present state of global wetland extent and wetland methane modelling: Conclusions from a model inter-comparison project (WETCHIMP). *Biogeosciences*, *10*(2), 753–788. https://doi.org/10.5194/bg-10-753-2013

Miller, S. M., Miller, C. E., Commane, R., Chang, R. Y. W., Dinardo, S. J., Henderson, J. M., et al. (2016). A multiyear estimate of methane fluxes in Alaska from CARVE atmospheric observations. *Global Biogeochemical Cycles*, *30*(10), 1441–1453. https://doi.org/10.1002/2016GB005419

Myhre, G., Shindell, D., Bréon, F.-M., Collins, W., Fuglestvedt, J., Huang, J., et al. (2013). Anthropogenic and natural radiative forcing. In T. F. Stocker, D. Qin, G.-K. Plattner, M. Tignor, S. K. Allen, J. Boschung, et al. (Eds.), *Climate change 2013: The physical science basis. Contribution of working group I to the fifth assessment report of the inter-governmental panel on climate change*. Cambridge, UK and New York, NY, US: Cambridge University Press.

Neelin, J. D., Chou, C., & Su, H. (2003). Tropical drought regions in global warming and El Niño teleconnections. *Geophysical Research Letters*, *30*(24), 1–4. https://doi.org/10.1029/2003GL018625

Pandey, S., Houweling, S., Lorente, A., Borsdorff, T., Tsivlidou, M., Bloom, A. A., et al. (2020). Using satellite data to identify the methane emission controls of South Sudan's wetlands. *Biogeosciences Discussions*, *2020*, 1–31. Retrieved from https://bg.copernicus.org/preprints/bg-2020-251/

Papa, F., Prigent, C., Aires, F., Jimenez, C., Rossow, W. B., & Matthews, E. (2010). Interannual variability of surface water extent at the global scale, 1993–2004. *Journal of Geophysical Research Atmospheres*, *115*(12), 1–17. https://doi.org/10.1029/2009JD012674

Parker, R., Webb, A., Boesch, H., Somkuti, P., Barrio Guillo, R., Di Noia, A., et al. (2020). A decade of GOSAT proxy satellite CH_4 observations. *Earth System Science Data Discussions*, 1–36. https://doi.org/10.5194/essd-2020-114

Pekel, J. F., Cottam, A., Gorelick, N., & Belward, A. S. (2016). High-resolution mapping of global surface water and its long-term changes. *Nature*, *540*(7633), 418–422. https://doi.org/10.1038/nature20584

Poulter, B., Bousquet, P., Canadell, J. G., Ciais, P., Peregon, A., Saunois, M., et al. (2017). Global wetland contribution to 2000-2012 atmospheric methane growth rate dynamics. *Environmental Research Letters*, *12*, 094013. https://doi.org/10.1088/1748-9326/aa8391

Riley, W. J., Subin, Z. M., Lawrence, D. M., Swenson, S. C., Torn, M. S., Meng, L., et al. (2011). Barriers to predicting changes in global terrestrial methane fluxes: Analyses using CLM4Me, a methane biogeochemistry model integrated in CESM. *Biogeosciences*, *8*(7), 1925–1953. https://doi.org/10.5194/bg-8-1925-2011

Rodgers, C. D. (2000). *Inverse Methods for Atmospheric Sounding. Series on Atmospheric, Oceanic and Planetary Physics* (Vol. 2). WORLD SCIENTIFIC. https://doi.org/10.1142/3171

Rosentreter, J. A., Borges, A. V., Deemer, B. R., Holgerson, M. A., Liu, S., Song, C., et al. (2021). Half of global emissions come from highly variable aquatic ecosystem sources. *Nature Geoscience*, *14*(4), 225–230. https://doi.org/10.1038/s41561-021-00715-2

Saunois, M., Bousquet, P., Poulter, B., Peregon, A., Ciais, P., Canadell, J. G., et al. (2016). The global methane budget 2000-2012. *Earth System Science Data*, *8*(2), 697–751. https://doi.org/10.5194/essd-8-697-2016

Saunois, M., Stavert, A. R., Poulter, B., Bousquet, P., Canadell, J. G., Jackson, R. B., et al. (2020a). The global methane budget 2000-2017. *Earth System Science Data*, *12*(3), 1561–1623. https://doi.org/10.5194/essd-12-1561-2020

Saunois, M., Stavert, A. R., Poulter, B., Bousquet, P., Canadell, J. G., Jackson, R. B., et al. (2020b). Supplemental data of the Global Carbon Project Methane Budget 2019 (Version 2.0) [Data set]. Global Carbon Project. https://doi.org/10.18160/GCP-CH4-2019

Schroeder, R., McDonald, K. C., Chapman, B. D., Jensen, K., Podest, E., Tessler, Z. D., et al. (2015). Development and evaluation of a multi-year fractional surface water data set derived from active/passive microwave remote sensing data. *Remote Sensing*, *7*(12), 16688–16732. https://doi.org/10.3390/rs71215843

Schuh, A. E., Jacobson, A. R., Basu, S., Weir, B., Baker, D., Bowman, K., et al. (2019). Quantifying the impact of atmospheric transport uncertainty on CO_2 surface flux estimates. *Global Biogeochemical Cycles*, *33*(4), 484–500. https://doi.org/10.1029/2018GB006086

Schuur, E. A. G., McGuire, A. D., Schädel, C., Grosse, G., Harden, J. W., Hayes, D. J., et al. (2015). Climate change and the permafrost carbon feedback. *Nature*, *520*(7546), 171–179. https://doi.org/10.1038/nature14338

Spahni, R., Joos, F., Stocker, B. D., Steinacher, M., & Yu, Z. C. (2013). Transient simulations of the carbon and nitrogen dynamics in northern peatlands: From the Last Glacial Maximum to the 21st century. *Climate of the Past*, *9*(3), 1287–1308. https://doi.org/10.5194/cp-9-1287-2013

Spahni, R., Wania, R., Neef, L., Van Weele, M., Pison, I., Bousquet, P., et al. (2011). Constraining global methane emissions and uptake by ecosystems. *Biogeosciences*, *8*(6), 1643–1665. https://doi.org/10.5194/bg-8-1643-2011

Tian, H., Lu, C., Ciais, P., Michalak, A. M., Canadell, J. G., Saikawa, E., et al. (2016). The terrestrial biosphere as a net source of greenhouse gases to the atmosphere. *Nature*, *531*(7593), 225–228. https://doi.org/10.1038/nature16946

Turner, A. J., Frankenberg, C., & Kort, E. A. (2019). Interpreting contemporary trends in atmospheric methane. *Proceedings of the National Academy of Sciences of the United States of America*, *116*(8), 2805–2813. https://doi.org/10.1073/pnas.1814297116

Turner, A. J., Jacob, D. J., Wecht, K. J., Maasakkers, J. D., Lundgren, E., Andrews, A. E., et al. (2015). Estimating global and North American methane emissions with high spatial resolution using GOSAT satellite data. *Atmospheric Chemistry and Physics*, *15*(12), 7049–7069. https://doi.org/10.5194/acp-15-7049-2015

Wania, R., Melton, J. R., Hodson, E. L., Poulter, B., Ringeval, B., Spahni, R., et al. (2013). Present state of global wetland extent and wetland methane modelling: Methodology of a model inter-comparison project (WETCHIMP). *Geoscientific Model Development*, *6*(3), 617–641. https://doi.org/10.5194/gmd-6-617-2013

Wenzel, S., Cox, P. M., Eyring, V., & Friedlingstein, P. (2016). Projected land photosynthesis constrained by changes in the seasonal cycle of atmospheric CO_2. *Nature*, *538*(7626), 499–501. https://doi.org/10.1038/nature19772

Widhalm, B., Bartsch, A., & Heim, B. (2015). A novel approach for the characterization of tundra wetland regions with C-band SAR satellite data. *International Journal of Remote Sensing*, *36*(22), 5537–5556. https://doi.org/10.1080/01431161.2015.1101505

Worden, J., Kulawik, S. S., Shephard, M. W., Clough, S. A., Worden, H., Bowman, K., & Goldman, A. (2004). Predicted errors of tropospheric emission spectrometer nadir retrievals from spectral window selection. *Journal of Geophysical Research*, *109*(D9), 1–12. https://doi.org/10.1029/2004jd004522

Yin, Y., Chevallier, F., Ciais, P., Bousquet, P., Saunois, M., Zheng, B., et al. (2020). Accelerating methane growth rate from 2010 to 2017: Leading contributions from the tropics and East Asia. *Atmospheric Chemistry and Physics Discussions*. [preprint], in review. https://doi.org/10.5194/acp-2020-649

Yvon-Durocher, G., Allen, A. P., Bastviken, D., Conrad, R., Gudasz, C., St-Pierre, A., et al. (2014). Methane fluxes show consistent temperature dependence across microbial to ecosystem scales. *Nature*, *507*(7493), 488–491. https://doi.org/10.1038/nature13164

Zhang, Y., Jacob, J. D., Lu, X., Maasakkers, D., Scarpelli, T. R., Sheng, J.-X., et al. (2021). Attribution of the accelerating increase in atmospheric methane during 2010–2018 by inverse analysis of GOSAT observations. *Atmospheric Chemistry and Physics*, *21*(5), 3643–3666. https://doi.org/10.5194/acp-21-3643-2021

Zhang, Z., Zimmermann, N. E., Calle, L., Hurtt, G., Chatterjee, A., & Poulter, B. (2018). Enhanced response of global wetland methane emissions to the 2015-2016 El Niño-Southern Oscillation event. *Environmental Research Letters*, *13*(7), 074009. https://doi.org/10.1088/1748-9326/aac939

Zhang, Z., Zimmermann, N. E., Stenke, A., Li, X., Hodson, E. L., Zhu, G., et al. (2017). Emerging role of wetland methane emissions in driving 21st century climate change. *Proceedings of the National Academy of Sciences of the United States of America*, *114*(36), 9647–9652. https://doi.org/10.1073/pnas.1618765114